Supplement of Geosci. Model Dev., 19, 11405–11418, 2026
https://doi.org/10.5194/gmd-19-11405-2026-supplement
© Author(s) 2026. CC BY 4.0 License.



Geoscientific Model Development
Open Access
EGU

Supplement of

Kinetic partitioning with effective mass accommodation for secondary organic aerosol simulations in chemical transport modeling

Regina Luu et al.

Correspondence to: Manabu Shiraiwa (m.shiraiwa@uci.edu)

The copyright of individual parts of the supplement might differ from the article licence.

Table S1. Molecular weight (MW) and glass transition temperature (T_g) for oxidation products in volatility bins. Values of MW and T_g correspond to the respective volatility bin.

	TSOA (Pai et al., 2020)	ASOA (Pai et al., 2020)
C^0 (μg m^{-3})	0.1	10^{-10}
	1	1
	10	10
	100	100

	TSOA (Shiraiwa et al., 2014)	ASOA (Shiraiwa et al., 2014; Shiraiwa et al., 2017)	LVOCOA (Shiraiwa et al., 2014)	SOAGX (Shiraiwa et al., 2014)
MW (g mol^{-1})	260	400	240	150
	240	362		
	220	249		
	200	227		

	TSOA	ASOA	LVOCOA	SOAIE (Chen et al., 2023)	SOAGX
T_g (K)	304	345*	314	231	261
	289	289			
	273	273			
	257	256			

T_g's calculated with T_g equation (Eq. (8)) except for SOAIE which was prescribed.

* Note that the volatility used to calculate the T_g for ASOAN is 10^{-4} μg m^{-3} in line with our previous study.

Table S2. Global averages of percent differences in SOA budget (between the α_{eff} kinetic and base case partitioning scheme simulations).

	Annual (%)	Winter (DJF) (%)	Spring (MAM) (%)	Summer (JJA) (%)	Autumn (SON) (%)
500 hPa	+14.56	+13.02	+14.31	+16.53	+15.97
850 hPa	1.43	+1.28	+1.78	+1.10	+1.97
Surface	-0.17	-0.03	+0.06	-0.06	+0.17
Total Column	-15.95	-17.57	-17.28	-15.10	-12.86

Table S3. Computational demand of 1-month benchmarked GEOS-Chem simulations, reported as wall-clock time (actual elapsed runtime), aggregate CPU time (summed CPU usage across cores), and maximum resident memory (MaxRSS).

Scheme	Wall-Clock Time (hh:mm:ss)	CPU Time (dd-hh:mm:ss)	MaxRSS (GB)
True Base [1]	06:37:31	17-16:01:04	5.87
"Base" [2]	06:40:45	17-19:28:00	5.87
α_{eff}	06:24:19	17-02:02:40	5.62

* Simulations were run on a single dedicated node using 64 CPU cores.

[1] The True Base scheme refers to the default complex scheme with no changes to the GEOS-Chem ver. 14.1.1 source code.

[2] The "Base" scheme refers the modified version of the complex scheme that includes volatility-dependent heat of vaporization parameterization which is used to compare to the α_{eff} in the main text**.**

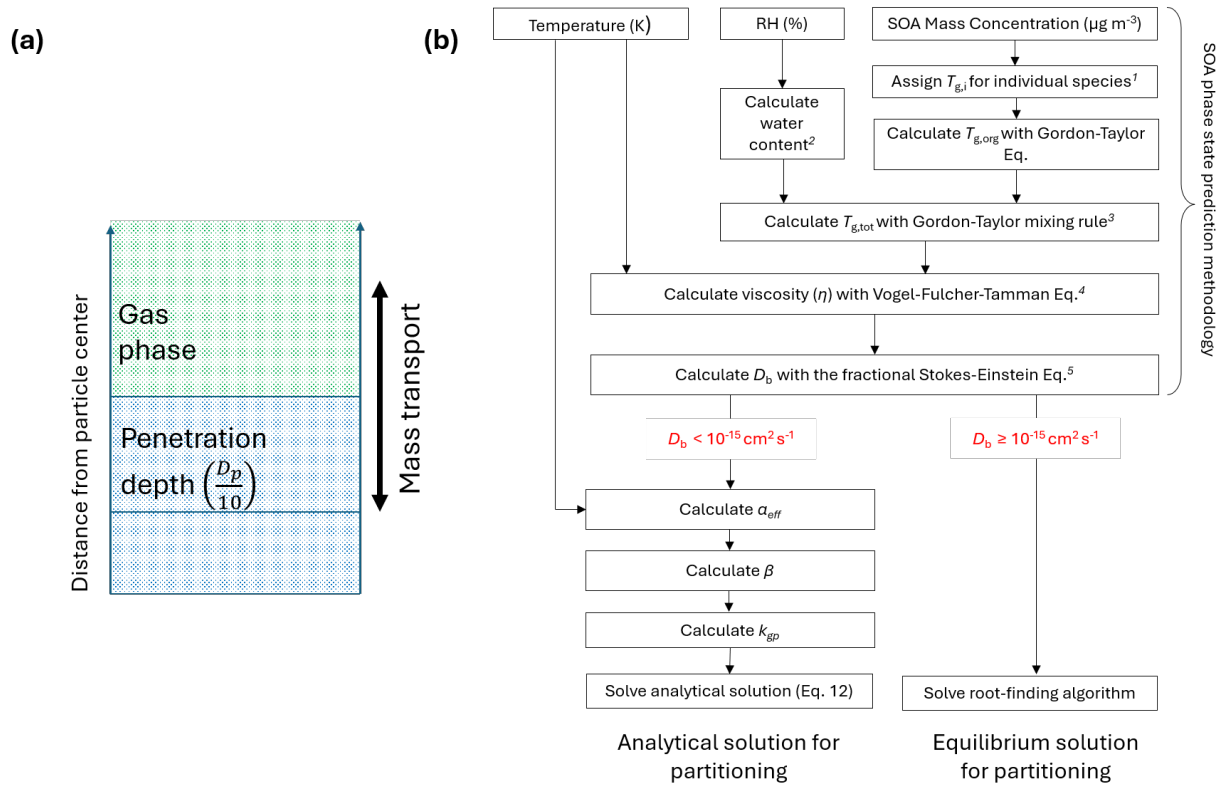

[1] $T_{g,i}$ for each species was calculated based on Eq. (8) and can be found in Table S1.
[2] The effective hygroscopicity parameter (κ) for SOA is assumed to be 0.1 (Lambe et al., 2011; Petters and Kreidenweis, 2007). The density of SOA particles (ρ_{SOA}) is assumed to be 1.4 g cm^{-3} (Cross et al., 2007).
[3] The glass transition temperature of pure water ($T_{g,w}$) is 136 K and the Gordon-Taylor constant for organic-water mixtures (k_{GT}) is assumed to be 2.5(Koop et al., 2011).
[4] The threshold between semi-solid and liquid states depends on the so-called fragility parameter (D) which is assumed to be 10(DeRieux et al., 2018).
[5] We assume that the hydrodynamic radius of a diffusing species is 0.38 nm and x is an empirical fit parameter determined to be 0.93(Evoy et al., 2019).

Figure S1. Modeling schematics of (a) the zero-dimensional box model simulating gas-particle partitioning solving Eq. (5, 6) using α_{eff} to govern reversible mass transport between the gas phase and the particle phase at the set penetration depth. The workflow chart for (b) the revised SOA partitioning scheme implemented in GEOS-Chem shows that environmental conditions and SOA mass concentration are used to calculate bulk diffusivity which is ultimately used to determine the partitioning approach.

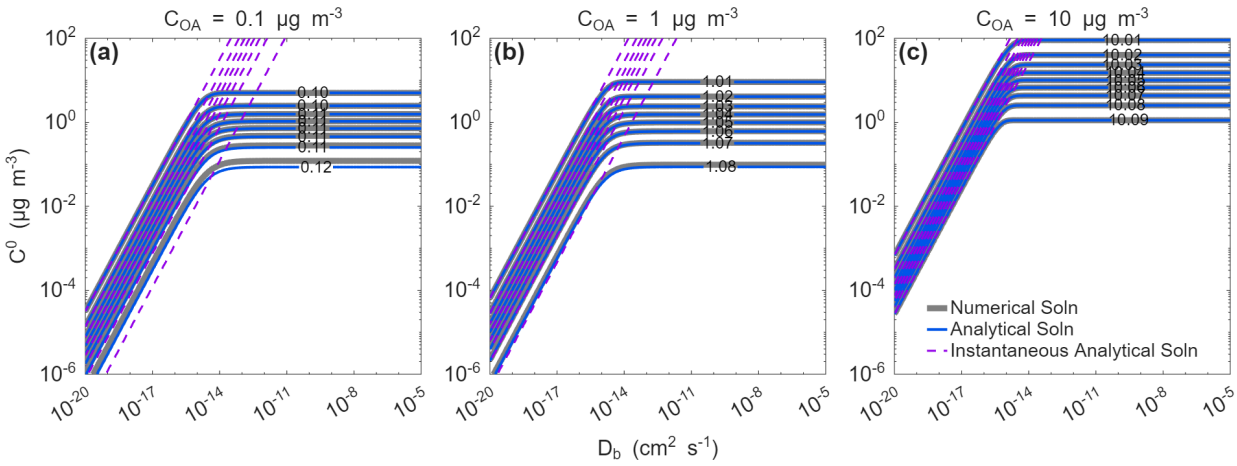

Figure S2. Contour plot of the final (t = 1200s) particle-phase concentration calculated using the (1) numerical, (2) analytical, and (3) analytical solution using the instantaneous conditions as a function of bulk diffusivity (D_b), saturation mass concentration (C^0), and initial pre-existing particle concentrations (C_{OA}) of (a) 0.1 µg m^{-3}, (b,) 1 µg m^{-3}, and (c) 10 µg m^{-3}. The initial gas-phase concentration was 0.1 µg m^{-3} and the temperature was set to 298K.

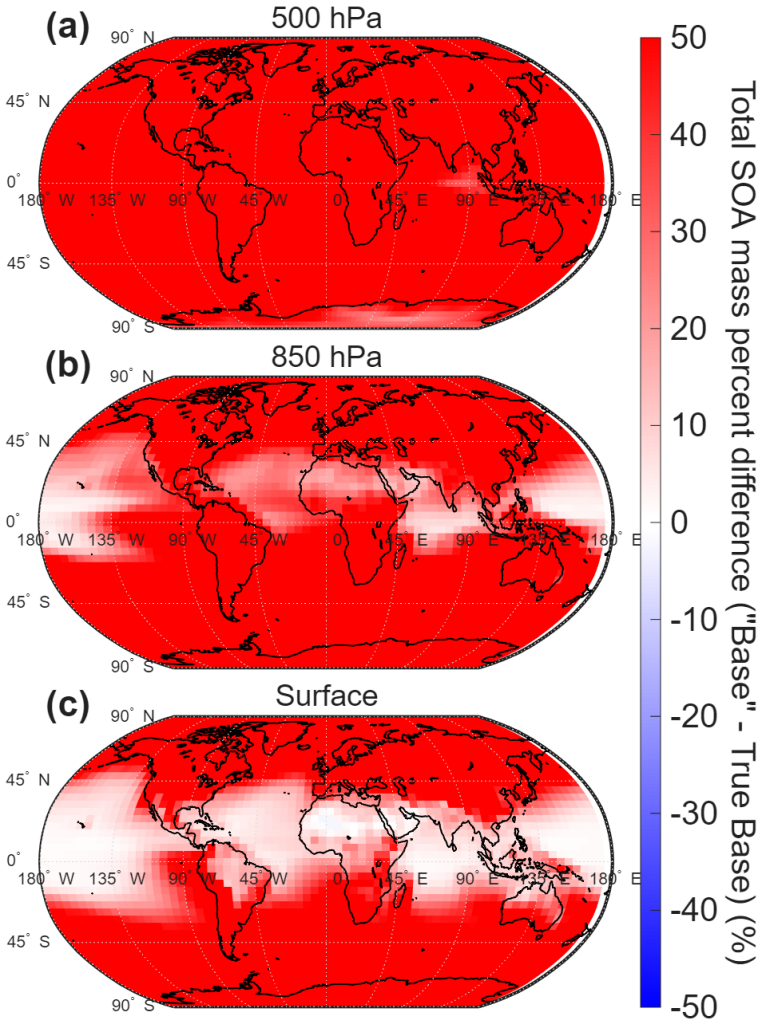

Figure S3. Annually averaged predicted percent SOA mass loading differences (a) at 500 hPa, (b) at 850 hPa, and (c) at the surface between the base case partitioning scheme and the true base simulations.

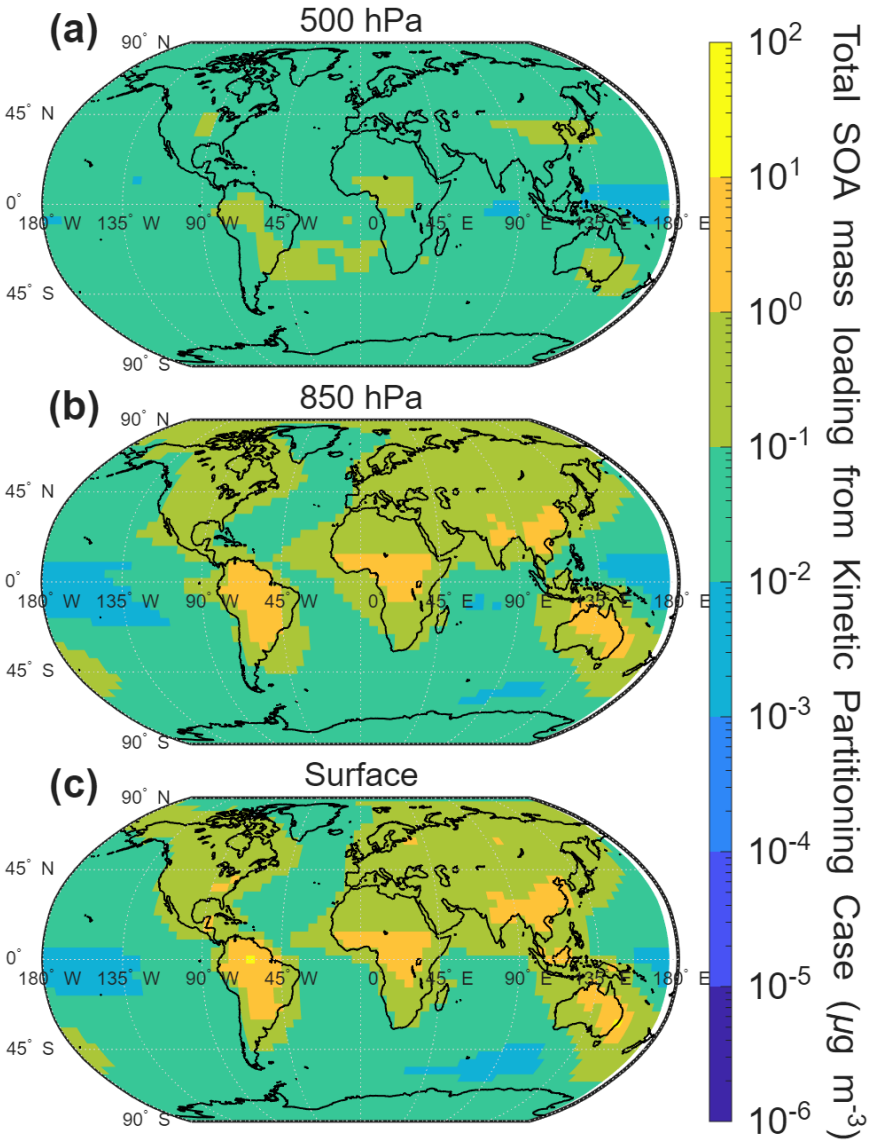

Figure S4. Predicted annual SOA budget (a) at 500 hPa, (b) at 850 hPa, and (c) at the surface using the α_{eff} kinetic partitioning scheme.

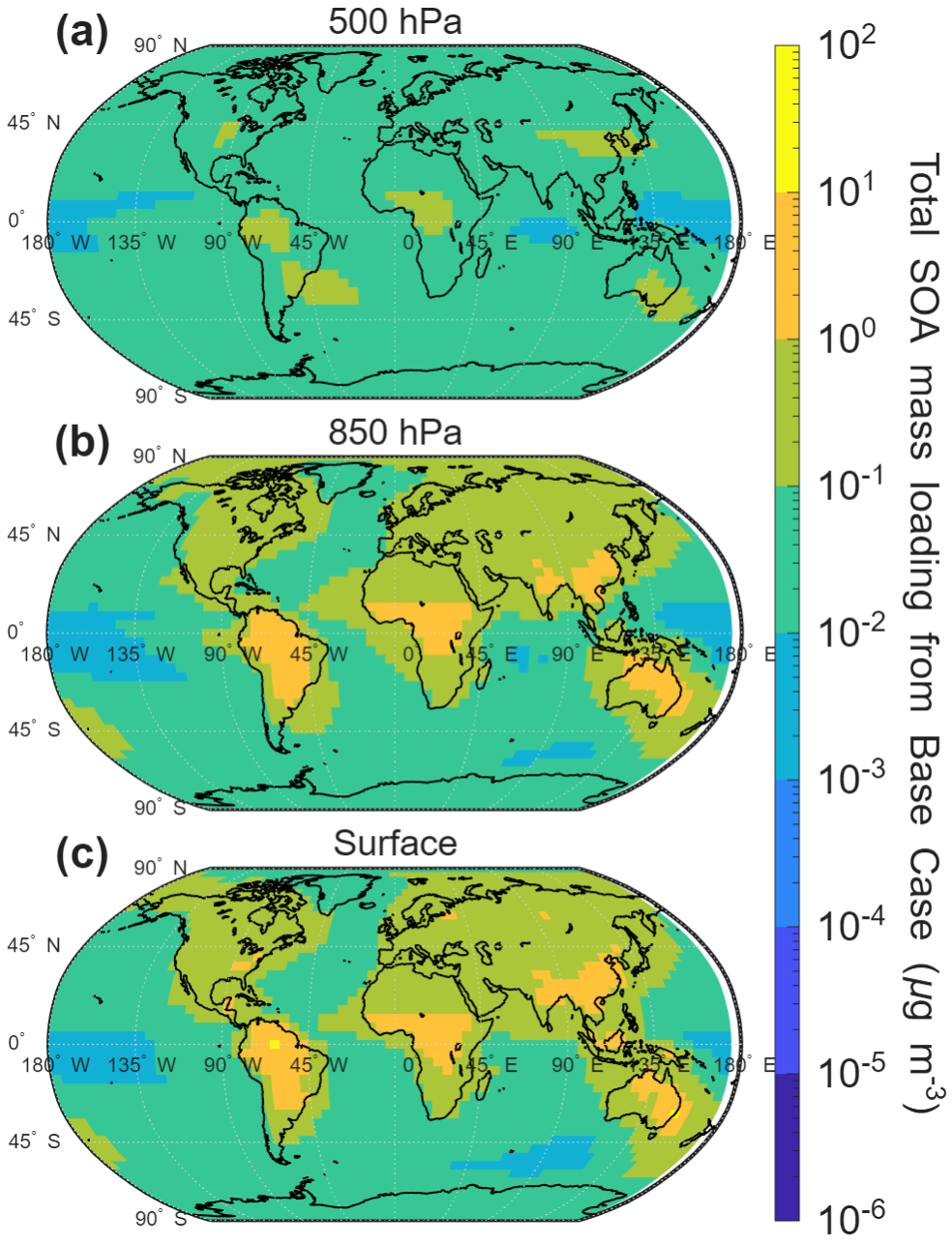

Figure S5. Predicted annual SOA budget (a) at 500 hPa, (b) at 850 hPa, and (c) at the surface using the Base case partitioning scheme.

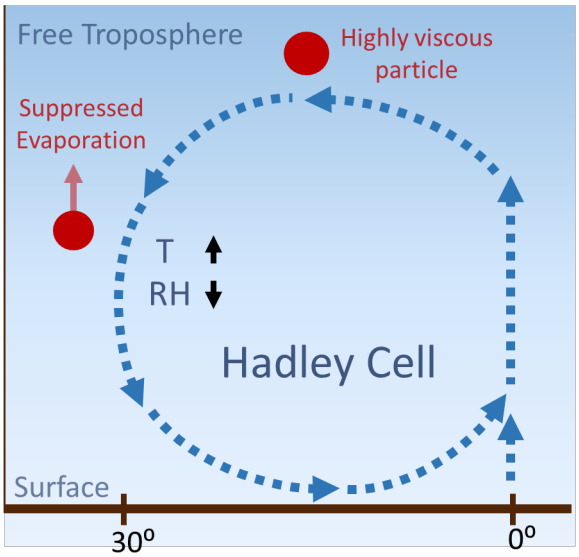

Figure S6. Schematic of Hadley Cell lifting highly viscous particles to the upper troposphere and transporting particles lower in altitude which would experience suppressed evaporation.

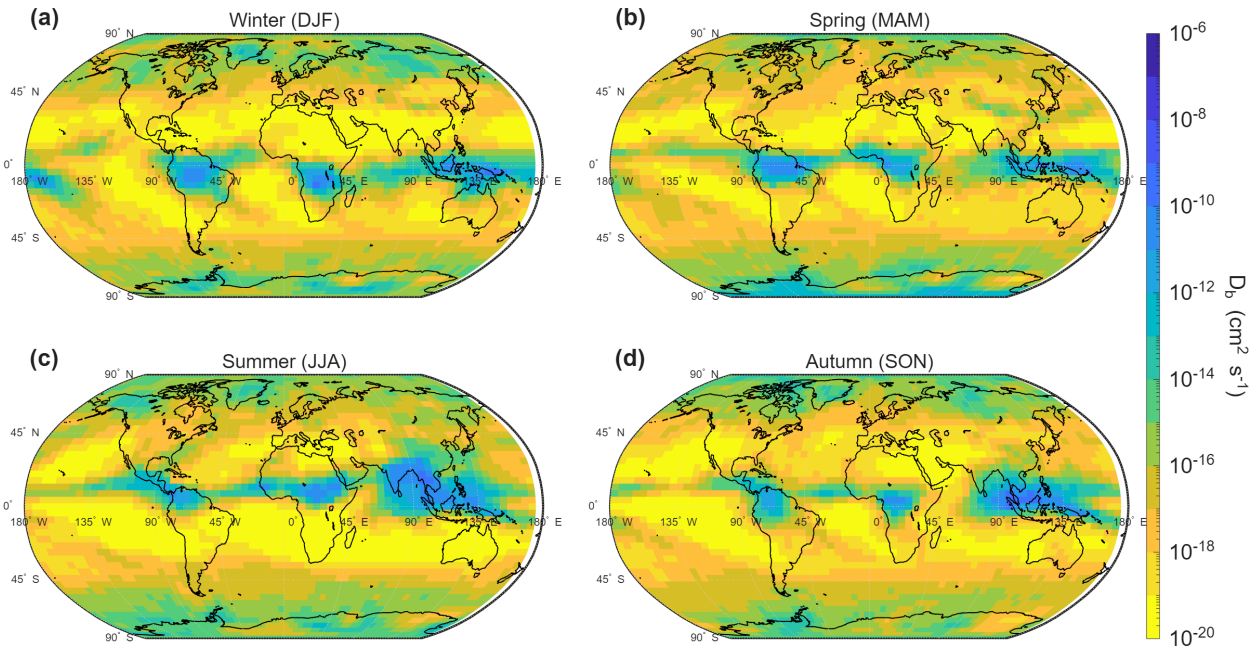

Figure S7. Predicted seasonal bulk diffusivities at 500 hPa.

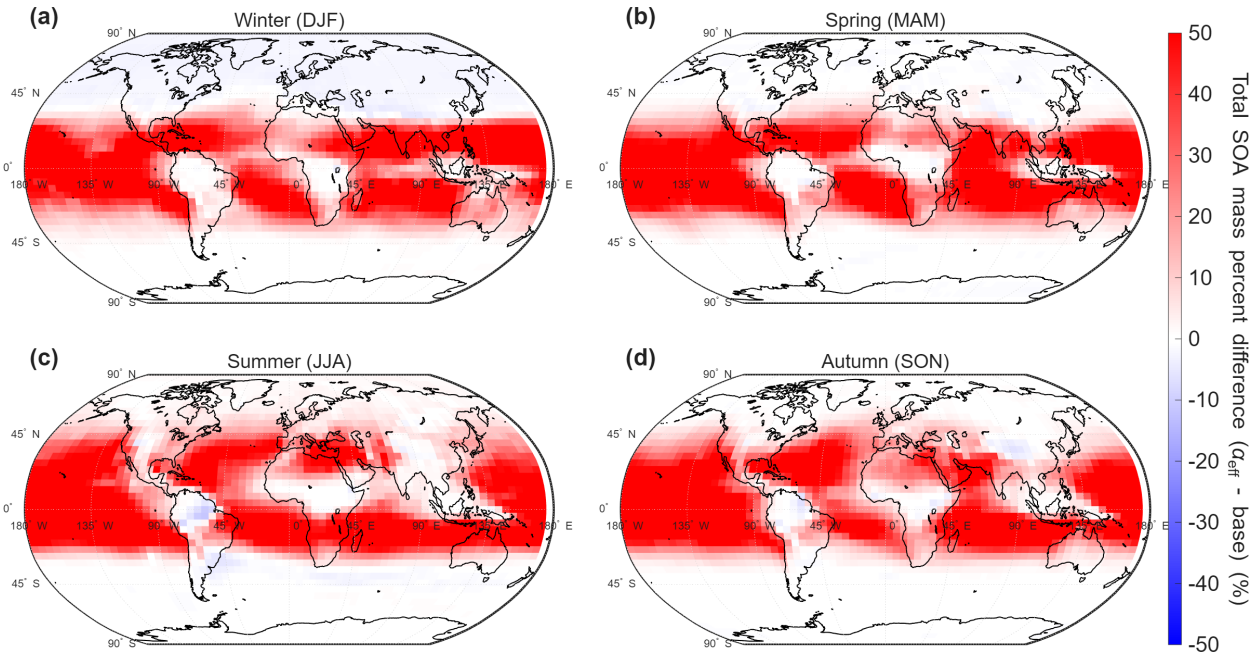

Figure S8. Predicted seasonal percent SOA budget differences at 500 hPa.

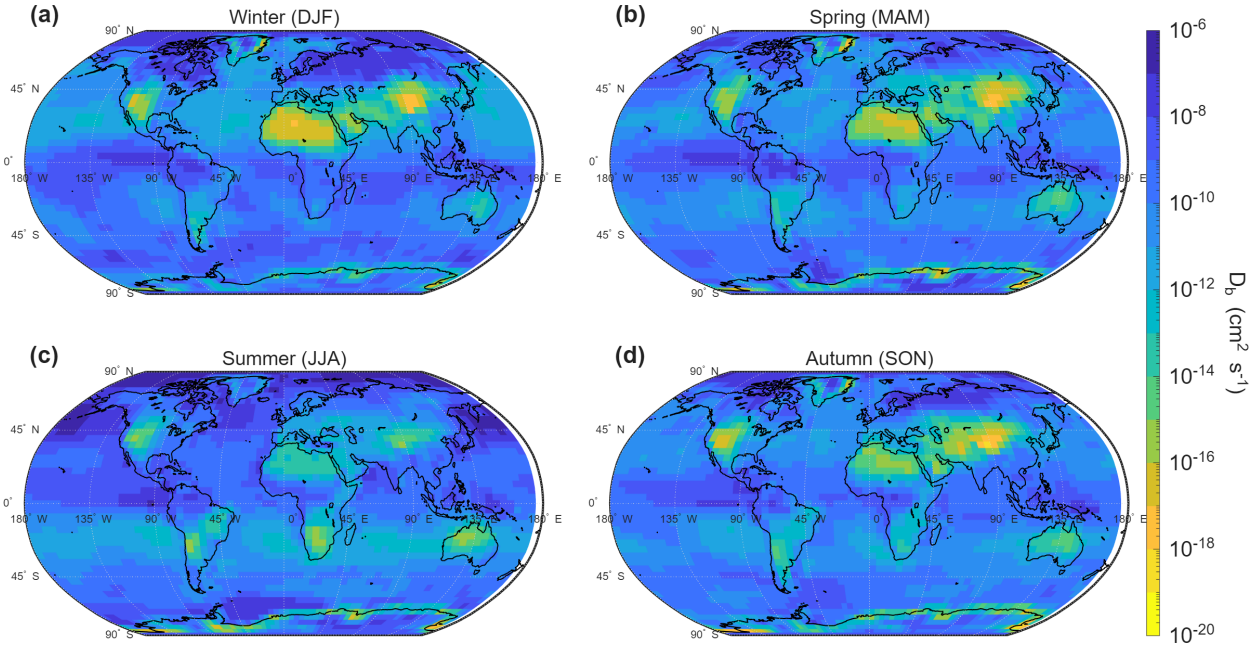

Figure S9. Predicted seasonal bulk diffusivities at the surface using the α_{eff} scheme.

References

Chen, B., Mirrielees, J. A., Chen, Y., Onasch, T. B., Zhang, Z., Gold, A., Surratt, J. D., Zhang, Y., and Brooks, S. D., Glass Transition Temperatures of Organic Mixtures from Isoprene Epoxydiol-Derived Secondary Organic Aerosol, The Journal of Physical Chemistry A, 127(18), 4125–4136, https://doi.org/10.1021/acs.jpca.2c08936, 2023.

Cross, E. S., Slowik, J. G., Davidovits, P., Allan, J. D., Worsnop, D. R., Jayne, J. T., Lewis †, D. K., Canagaratna, M., and Onasch, T. B., Laboratory and Ambient Particle Density Determinations using Light Scattering in Conjunction with Aerosol Mass Spectrometry, Aerosol Science and Technology, 41(4), 343–359, https://doi.org/10.1080/02786820701199736, 2007.

DeRieux, W.-S. W., Li, Y., Lin, P., Laskin, J., Laskin, A., Bertram, A. K., Nizkorodov, S. A., and Shiraiwa, M., Predicting the glass transition temperature and viscosity of secondary organic material using molecular composition, Atmospheric Chemistry and Physics, 18(9), 6331–6351, https://doi.org/10.5194/acp-18-6331-2018, 2018.

Evoy, E., Maclean, A. M., Rovelli, G., Li, Y., Tsimpidi, A. P., Karydis, V. A., Kamal, S., Lelieveld, J., Shiraiwa, M., Reid, J. P., and Bertram, A. K., Predictions of diffusion rates of large organic molecules in secondary organic aerosols using the Stokes–Einstein and fractional Stokes–Einstein relations, Atmospheric Chemistry and Physics, 19(15), 10073–10085, https://doi.org/10.5194/acp-19-10073-2019, 2019.

Koop, T., Bookhold, J., Shiraiwa, M., and Pöschl, U., Glass transition and phase state of organic compounds: dependency on molecular properties and implications for secondary organic aerosols in the atmosphere, Physical Chemistry Chemical Physics, 13(43), 19238–19255, https://doi.org/10.1039/C1CP22617G, 2011.

Lambe, A. T., Onasch, T. B., Massoli, P., Croasdale, D. R., Wright, J. P., Ahern, A. T., Williams, L. R., Worsnop, D. R., Brune, W. H., and Davidovits, P., Laboratory studies of the chemical composition and cloud condensation nuclei (CCN) activity of secondary organic aerosol (SOA) and oxidized primary organic aerosol (OPOA), Atmospheric Chemistry and Physics, 11(17), 8913–8928, https://doi.org/10.5194/acp-11-8913-2011, 2011.

Pai, S. J., Heald, C. L., Pierce, J. R., Farina, S. C., Marais, E. A., Jimenez, J. L., Campuzano-Jost, P., Nault, B. A., Middlebrook, A. M., Coe, H., Shilling, J. E., Bahreini, R., Dingle, J. H., and Vu, K., An evaluation of global organic aerosol schemes using airborne observations, Atmospheric Chemistry and Physics, 20(5), 2637–2665, https://doi.org/10.5194/acp-20-2637-2020, 2020.

Petters, M. D., and Kreidenweis, S. M., A single parameter representation of hygroscopic growth and cloud condensation nucleus activity, Atmospheric Chemistry and Physics, 7(8), 1961–1971, https://doi.org/10.5194/acp-7-1961-2007, 2007.

Shiraiwa, M., Berkemeier, T., Schilling-Fahnestock, K. A., Seinfeld, J. H., and Pöschl, U., Molecular corridors and kinetic regimes in the multiphase chemical evolution of secondary organic aerosol, Atmospheric Chemistry and Physics, 14(16), 8323–8341, https://doi.org/10.5194/acp-14-8323-2014, 2014.

Shiraiwa, M., Li, Y., Tsimpidi, A. P., Karydis, V. A., Berkemeier, T., Pandis, S. N., Lelieveld, J., Koop, T., and Pöschl, U., Global distribution of particle phase state in atmospheric secondary organic aerosols, Nature Communications, 8(1), 15002, https://doi.org/10.1038/ncomms15002, 2017.